Journal of
Materials Chemistry C

RSC Publishing

PAPER

View Article Online
View Journal | View Issue

Open Access Article. Published on 29 January 2013. Downloaded on 12/15/2025 9:26:05 AM.
This article is licensed under a Creative Commons Attribution 3.0 Unported Licence.

Cite this: *J. Mater. Chem. C*, 2013, **1**, 2433

Polythiophene–perylene diimide heterojunction field-effect transistors†

Sreenivasa Reddy Puniredd,‡[a] Adam Kiersnowski,[ab] Glauco Battagliarin,[a] Wojciech Zajączkowski,[a] Wallace W. H. Wong,[c] Nigel Kirby,[d] Klaus Müllen*[a] and Wojciech Pisula§*[a]

Received 5th November 2012
Accepted 27th January 2013

DOI: 10.1039/c3tc00562c

www.rsc.org/MaterialsC

Thin film field-effect transistors based on binary blends of poly(3-hexylthiophene) (P3HT) and two perylene diimide (PDI) derivatives with different alkyl substituents have been investigated in terms of device performance, microstructure and molecular organization on the surface. For the same blend ratios the PDIs phase separate differently due to solubility variation. Blends with a horizontal phase separation between the donor and acceptor show ambipolar behavior due to well defined homogenous pathways for both charge carriers. In this layer arrangement the polymer is located near the dielectric interface, while the PDI molecules crystallize on top of the film. Interestingly, the electron mobility is improved by a few orders of magnitude in comparison to the pure acceptor. This increase is attributed to the altered microstructure of PDI in the blends. Layers in which the PDI crystals are embedded within the polymer matrix and are not interconnected with each other lead only to hole transport in the transistor. For one blend ratio, the hole mobility improves by one order of magnitude compared to pure P3HT as a result of the reorganization of the polymer in the blend layer. This study provides new insights into the role of microstructure and molecular organization in the charge carrier transport in heterojunction field-effect transistors for the development of high-performance future devices.

Introduction

Organic field-effect transistors (FETs) based on solution processable conjugated polymers are technologically attractive as active components in cheap and flexible electronic devices such as radio frequency identification (RF-ID) tags and active matrix of flexible displays.[1] Most recent high-performance polymeric organic semiconductors revealed unipolar device operation,[2] while an ambipolar transport of electrons and holes is required for applications in complementary-like logic circuits.[3] The main reasons for unipolarity are unoptimized device geometries and molecular energy levels suited for only one type of charge carrier.[4]

There are several approaches to build ambipolar transistors. The simplest method is based on the separate deposition of p- and n-type materials on the corresponding electrodes of the logic circuit.[5] However, this procedure involves complex and precise solution deposition techniques. Recently, single-component transistors with ambipolar behavior have been reported reaching high balanced mobilities.[6] The optimization of the molecular design towards ambipolarity is a challenging task and the synthesis often remains a complicated multistep procedure. An alternative is the employment of a mixture of two components having different electronic affinity which form a heterojunction blend in the active layer after solution deposition.[7] The heterojunction structure depends on the deposition conditions and can vary between a simple bilayer[8] and a complex interdigitation[9] of both phases. Intensive studies have been performed on the effect of the heterojunction microstructure on the efficiency of organic photovoltaics.[10] Such bulk heterostructures are highly attractive due to their expanded interface between the donor and acceptor available for charge separation, which can overcome the limits of short exciton diffusion length in organic semiconductors in photovoltaics.[11] Since the charge carrier migration in FETs occurs parallel to the substrate, the bulk heterostructure interface needs to be adapted accordingly to avoid scattering of charges and interruption in the charge carrier pathway. The microstructure plays a crucial role in determining the device properties due to the

[a]*Max Planck Institute for Polymer Research, Ackermannweg 10, 55128 Mainz, Germany. E-mail: pisula@mpip-mainz.mpg.de; muellen@mpip-mainz.mpg.de; Fax: +49 6131-379-350; Tel: +49 6131-379-151*

[b]*Wroclaw University of Technology, Polymer Engineering and Technology Division, Wybrzeze Wyspianskiego 27, 50-370 Wroclaw, Poland*

[c]*School of Chemistry, Bio21 Institute, University of Melbourne, 30 45 Flemington Road, Parkville, Victoria 3010, Australia*

[d]*Australian Synchrotron, 800 Blackburn Road, Clayton, Victoria 3168, Australia*

† Electronic supplementary information (ESI) available. See DOI: 10.1039/c3tc00562c

‡ Present address: Institute of Materials Research and Engineering, A*Star, 3 Research Link, Singapore, 117602.

§ Present address: Evonik Industries AG, Kirschenallee, 64293 Darmstadt, Germany.

Open Access Article. Published on 29 January 2013. Downloaded on 12/15/2025 9:26:05 AM.
This article is licensed under a Creative Commons Attribution 3.0 Unported Licence.

requirement of each semiconductor to contact the source and drain electrodes and to form sufficient percolation paths for each type of charge carrier.[12] Therefore, it is a great challenge to precisely control the direction and length scale of such phase-separated microstructures for transistor applications since this limits the electronic functionality of the blend film. The phase separation can occur either horizontally or vertically with respect to the surface. For an unhindered charge migration the corresponding electron or hole transporting fractions should connect the source and drain electrodes. Additionally, the transport of holes and electrons through the corresponding phases can be improved by increasing the local molecular order and crystallinity.[13]

The most prominent acceptor used in bulk heterojunction photovoltaics is PCBM ([6,6]-phenyl C61-butyric acid methyl-ester) due to the match of its energy levels to many donor materials and due to its excellent electron transporting properties.[14] PCBM has also been successfully applied for many heterojunction FET devices in combination with various polymers and small molecules.[9] Recently, we have demonstrated perylene diimide (PDI) derivatives as an alternative for electron acceptors in heterojunction photovoltaics in combination with poly(3-hexylthiophene) (P3HT)[15] due to their strong absorption in the visible light region and typically high electron charge carrier mobilities.[16] The PDI derivatives are a promising electron transporting material for their exploitation in solution processed heterojunction FETs.

Therefore, in this work heterojunction ambipolar transistors with the active layer based on crystalline PDI and P3HT are studied and correlations between blend composition, heterojunction microstructure, molecular order and charge carrier transport of holes and electrons are established. While P3HT is a p-type conjugated polymer with well-known electronic properties and organization,[17] two PDI derivatives with different alkyl substituents and solubility are investigated leading to altered organization in the blended thin layers. This study indicates that the layer location near the dielectric interface plays a crucial role in the device operation. Interestingly, for few blend ratios the charge carrier mobility significantly improves in comparison to the pure compounds. As with our previous studies on photovoltaics, this work provides a further insight into the ambipolar charge carrier transport mechanism in heterojunctions.

Results and discussion

The chemical structures of the investigated PDI derivatives are depicted in Scheme 1. Compound PDI-2 was specifically designed to increase the solubility by additional bulky alkyl side chains in comparison to PDI-1. As the donor, P3HT with a regioregularity of ~94%, $M_w = 60$ kg mol^{-1} and PDI = 2.2 was used.

The transport behavior of hole and electron carriers was investigated by FET measurements. Bottom-contact, bottom-gate hexamethyldisilazane (HMDS) treated devices were fabricated by spin coating a chloroform solution at a concentration of 10 mg ml^{-1} of the pure compounds and the mixtures. After deposition, the thin films were annealed at 120 °C for 20 min. Three blend ratios for each PDI derivative have been investigated: 1 : 1, 1 : 3 and 3 : 1 (w/w) P3HT:PDI.

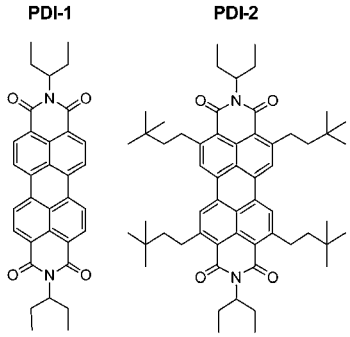

Scheme 1 Chemical structures of the investigated PDI derivatives. PDI-1 bears short branched alkyl-chains at the *N*-imide position. PDI-1 served as the starting material for the synthesis of PDI-2, which carries additional bulky alkyl-substituents at the 2-, 5-, 8-, and 11-position of the PDI core.

A moderate p-type saturation mobility of 3.7×10^{-2} cm^2 V^{-1} s^{-1} was determined for pure P3HT (Table 1), which is typical for spin-coated thin P3HT layers.[18] The microstructure of P3HT was inspected by atomic force microscopy (AFM), which reveals a uniform topography consisting of a nodular structure (Fig. 1a). This has been observed previously for P3HT samples with a similar molecular weight range.[19] Additional grazing incidence wide-angle X-ray scattering (GIWAXS) measurements on the film provide information about the organization of P3HT on the surface. The scattering maximum located on the meridian (Fig. S1,† $q_z \approx 1.64$ Å^{-1} at $q_{x,y} = 0$ Å^{-1} indicating a π-stacking distance of $d_\pi = 3.83$ Å) is a result of diffraction of X-rays on π-stacked polymer chains. The azimuthal location of this peak points towards a face-on orientation of the macromolecules

Table 1 Charge carrier mobility data derived from FET measurements for pure P3HT, PDI-1 and PDI-2 and blends of P3HT:PDI-1 and P3HT:PDI-2

Sample	$\mu_{h,sat}$ (cm^2 V^{-1} s^{-1})	$\mu_{e,sat}$ (cm^2 V^{-1} s^{-1})
P3HT	3.7×10^{-2}	—
PDI-1	—	1.1×10^{-6}
1 : 3 P3HT:PDI-1	1×10^{-3}	—
1 : 1 P3HT:PDI-1	4.5×10^{-3}	6×10^{-3}
3 : 1 P3HT:PDI-1	3×10^{-3}	2×10^{-5}
PDI-2	—	10^{-8}
1 : 3 P3HT:PDI-2	7×10^{-3}	2×10^{-3}
1 : 1 P3HT:PDI-2	2×10^{-3}	—
3 : 1 P3HT:PDI-2	0.1	—

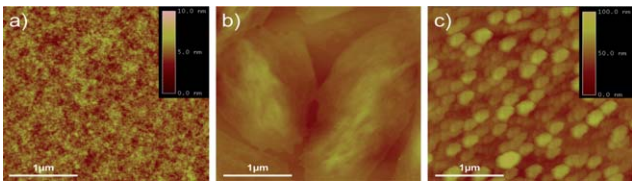

Fig. 1 AFM height images of spin-coated and annealed (at 120 °C for 20 min) (a) P3HT, (b) PDI-1 and (c) PDI-2 (height scale valid for both PDI derivatives).

Open Access Article. Published on 29 January 2013. Downloaded on 12/15/2025 9:26:05 AM.
This article is licensed under a Creative Commons Attribution 3.0 Unported Licence.

(Fig. 2a). It is known that the regioregularity of P3HT determines the polymer arrangement towards the surface and that P3HT with a relatively low regioregularity tends to organize in a face-on manner.[20] Further, distinct equatorial reflections at $q_{x,y} = 0.37$ Å^{-1} are related to the lateral chain-to-chain distance of 16.9 Å of the face-on organized polymer. Interestingly, the identical position of scattering maxima visible on the meridian at $q_z = 0.37$ Å^{-1} may be assigned to a certain fraction of P3HT with an edge-on arrangement (Fig. S1†). A very low intensity of equatorial reflections located at $q_{x,y} = 1.64$ Å^{-1} suggests, however, a significantly smaller amount of the edge-on oriented fraction which has additionally a shorter coherence length in the π-stacking direction. It can be therefore assumed that the polymer is organized in an edge-on and face-on manner: a major part of P3HT forms well-developed domains containing face-on oriented, π-stacked macromolecules while a smaller part is oriented edge-on towards the substrate with rather random organization in the direction normal to the aromatic planes. In the face-on arrangement of P3HT the insulating alkyl side chains are oriented in the same plane and lead to a lower charge carrier transport in the transistor. On the other hand, a face-on arrangement is considered to favor the solar cell efficiency since in this kind of device the main charge carrier direction is normal to the surface. Additional temperature dependent *in situ* GIWAXS measurements indicate that thermal annealing enhances both coherence of macromolecules within stacks (in other words: longer coherence length) and also ordering of stacks with respect to the surface (Fig. S2†).

As expected, both pure PDI-1 and PDI-2 show n-type behavior with low electron mobilities of 10^{-6} and 10^{-8} cm^2 V^{-1} s^{-1}, respectively (Table 1). It has to be mentioned that PDI-1 gives rise to more distinct output curves in comparison to PDI-2 which shows a very low field-effect (10^{-8} cm^2 V^{-1} s^{-1}). The low performance of both PDIs, and especially of PDI-2, can be explained in terms of their crystal size and order in the thin layer. AFM images of PDI-1 show several micrometer large leaf-like crystalline structures (Fig. 1b), while PDI-2 forms uniform grains of ~0.25 μm in average size (Fig. 1c). The small grain size and lower crystallinity of PDI-2 in comparison to PDI-1 can be attributed to the bulky side chains at the bay of the core which hinder molecular interactions in solution, reduce the self-assembly and thus lead to small domains. In both cases, the domains are obviously separated from each other by distinct grain boundaries which are known to limit the charge carrier transport in thin layers.[21] Equatorial reflections at $q_{x,y} = 1.85$ Å^{-1} in the GIWAXS pattern for PDI-1 are assigned to the π-stacking distance of 3.4 Å and indicate an edge-on arrangement of the molecules on the surface (Fig. 2b and S1†). Accordingly, the columnar stacks are oriented parallel to the surface as implied by the most intense reflection located on the meridional plane (located on the q_z axis) of the pattern. Unfortunately, due to insufficient number of peaks, the precise assignment of the 2D intercolumnar unit cell is impossible. Additional diffraction maxima visible at various azimuthal angles in the low to middle q-range result from a complex helical intracolumnar packing of the molecules within the columnar stacks, which has been already reported for other PDI derivatives in bulk and in thin layers.[22] In contrast to PDI-1, the pattern of PDI-2 is less complex and is characteristic for poorly developed microstructures (Fig. 2c). Nearly uniform, broad rings located at q-values ranging approximately from 1.1 Å^{-1} to 1.5 Å^{-1} indicate low crystallinity and mostly isotropic arrangement of molecules in the film. These GIWAXS results for PDI-2 are in agreement with the microstructure observed by AFM and the low FET performance. The bulky side chains of PDI-2 lower the molecular interactions and lead to a less ordered film as confirmed additionally by the lack of further reflections such as from π-stacking.

The device behavior of P3HT:PDI-1 and P3HT:PDI-2 blends was determined for three weight ratios of components: 1 : 3, 1 : 1 and 3 : 1. Clear ambipolar behavior for P3HT:PDI-1 1 : 1 is observed from the transfer curves in both p-type and n-type operation modes for positive and negative gate voltages with a hole and electron mobility of $\mu_h = 4.5 \times 10^{-3}$ cm^2 V^{-1} s^{-1} and $\mu_e = 6.0 \times 10^{-3}$ cm^2 V^{-1} s^{-1} (Fig. 3c and d). In the negative drain mode, $V_{DS} < 0$ V, the crossover point from electron- to hole-dominated current is at approximately $V_g = -25$ V (Fig. 3c). Below this gate voltage, the transistor shows a typical p-type behavior in the accumulation mode. On the other hand, in the

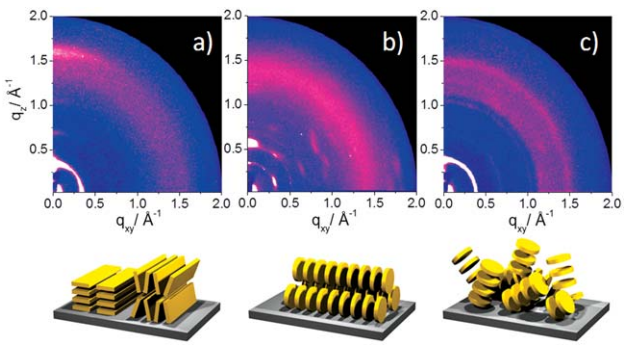

Fig. 2 GIWAXS patterns of thin films and the corresponding illustrations of the organization (alkyl substituents and helical rotation are omitted due to simplicity) of (a) P3HT, (b) PDI-1 and (c) PDI-2.

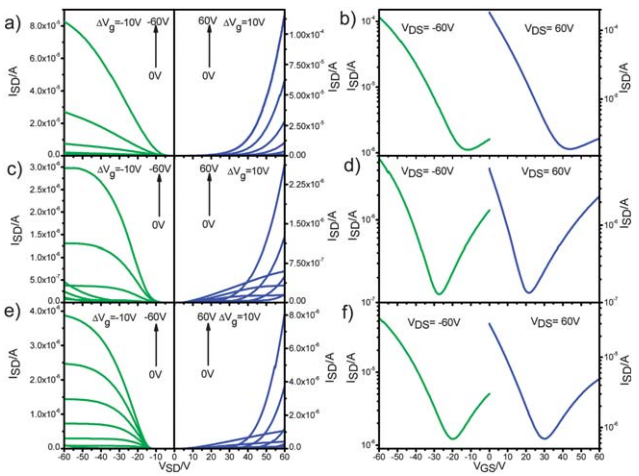

Fig. 3 Output and transfer FET characteristics for the P3HT:PDI-1 blends: (a and b) 1 : 3, (c and d) 1 : 1, and (e and f) 3 : 1.

Open Access Article. Published on 29 January 2013. Downloaded on 12/15/2025 9:26:05 AM.
This article is licensed under a Creative Commons Attribution 3.0 Unported Licence.

positive regime, $V_{DS} > 0$ V, electron domination and n-type properties of the device are obvious from $V_g = 20$ V. The symmetric form of the transfer characteristics in the saturation regime confirms a well-balanced transport of hole and electron carriers (Fig. 3d) and implies that the active film consists of phase separated donor and acceptor components. Interestingly, the electron mobility is significantly higher in comparison to the pure acceptor (PDI-1), while the value for holes drops by one order of magnitude in regard to the mobility of P3HT. For p-type systems, it has been previously observed that the performance of small crystalline oligomers can be improved by blending with conjugated polymers in small amounts. Thereby, the small molecules form crystals within the phase separated polymer thin layer.[23] However, it has not been reported so far for FETs that a p-type polymer can enhance the performance of an n-type small molecule (or *vice versa*), as it is the case for the current P3HT:PDI systems.

The increase of the donor fraction in the active layer for P3HT:PDI-1 3 : 1 reduces the electron transport leading to a mobility of only 2×10^{-5} cm^2 V^{-1} s^{-1}, while the hole value remains almost unchanged in comparison to the 1 : 1 ratio. Both output and transfer curves also show ambipolar device characteristics (Fig. 3f and g) whereby the electron transport in the p-type regime is less pronounced. This is also obvious for the less symmetric transfer plots (Fig. 3f). It has to be noted that in the p-type operation mode for $V_{DS} < 0$ V only a slight electron transport occurs most probably due to significant trapping of these charge carriers. Surprisingly, an increase of the acceptor fraction in the film to P3HT:PDI-1 1 : 3 yields only a unipolar behavior with holes as the main charge carriers in both operation modes (Fig. 3a) and mobilities of $\mu_h = 1 \times 10^{-3}$ cm^2 V^{-1} s^{-1} as extracted from the transfer curves (Fig. 3b). In the n-type operation regime, only diode-like curves are recorded indicating no electron transport.

To understand the electron and hole transport in the thin layer for different P3HT:PDI-1 blend ratios, the microstructure and molecular organization were investigated and compared to those of the pure compounds. Interestingly, the crystal microstructure of PDI-1 changes in the presence of P3HT as particularly evident from the AFM and scanning electron microscopy (SEM) images in Fig. 4b and 5b for P3HT:PDI-1 1 : 1 and in Fig. 5c and 6c for P3HT:PDI-1 3 : 1. In comparison to pure PDI-1, the sizes of 1.5–2.0 μm of the rod-shaped crystals are smaller, but have more regular shapes. The phase image shows that these crystals are distributed on top of the P3HT layer suggesting a bilayer with a horizontal phase separation between the donor and acceptor as it is also clearly evident from the cross-sectional SEM image (Fig. 5b). This spontaneous separation is in agreement with other blends containing PDI or other crystalline small molecules which preferentially crystallize at the top surface of spin-cast films.[24] By comparison, cross-sectional SEM images of annealed P3HT:PCBM exhibit a homogenous film microstructure due to the mutual miscibility and diffusion of the components.[25] Since the top and bottom layers are continuous for the 1 : 1 P3HT:PDI-1 ratio, a balanced transport of both types of charge carriers is observed in the transistor. Thereby, the PDI-1 crystals in the top layer are densely packed

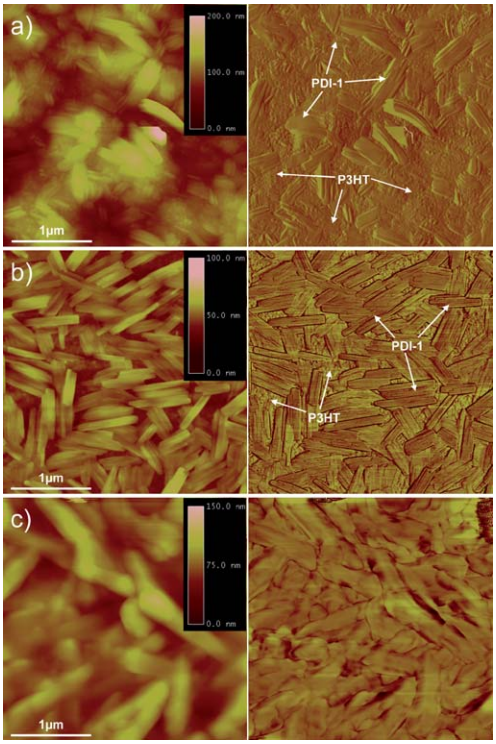

Fig. 4 AFM height (left) and phase (right) images for P3HT:PDI-1 blend films with the weight ratios of (a) 1 : 3, (b) 1 : 1, and (c) 3 : 1.

creating an interconnection for the electron transport and not directly linked to the dielectric interface where the main charge migration takes place.

The change of the PDI fraction has an unexpected effect on the microstructure of the film. Lowering the PDI-1 content in the film to 3 : 1 P3HT:PDI-1 increases the film area covered by PDI-1 crystals (Fig. 4c), whereby it has to be mentioned that the AFM image acquisition of this topography was challenging. In the height image the crystals are blurred and appear in low contrast (Fig. 4c). The reason is evident from the SEM image (Fig. 5c) which reveals again a vertically phase separated layer, but with PDI-1 crystals which partly stick out of the film up to 0.5 μm in height. Nevertheless, the necessary percolation pathways for electrons are established by the remaining PDI-1 crystals on top of the P3HT layer leading to a mobility of 2×10^{-5} cm^2 V^{-1} s^{-1}. Interestingly, increasing the PDI-1 content to 1 : 3 P3HT:PDI-1 decreases the PDI crystal concentration in the top layer of the active film (Fig. 4a). The AFM image clearly exhibits the PDI-1 crystals of *ca.* 1.5–2 μm in size on top of the P3HT matrix suggesting that the rest of the PDI-1 material should be embedded in the bulk film. This is indeed confirmed by the cross-sectional SEM image in which PDI-1 crystals are vertically embedded within the continuous P3HT matrix (Fig. 5a). This distribution of the crystals hinders an interconnection between PDI-1 domains, lowers possible in-plane electron percolation and thus blocks the electron transport through the layer.

To confirm the phase separation between P3HT and PDI-1 in the thin film and to inspect the molecular organization in the

Open Access Article. Published on 29 January 2013. Downloaded on 12/15/2025 9:26:05 AM.
This article is licensed under a Creative Commons Attribution 3.0 Unported Licence.

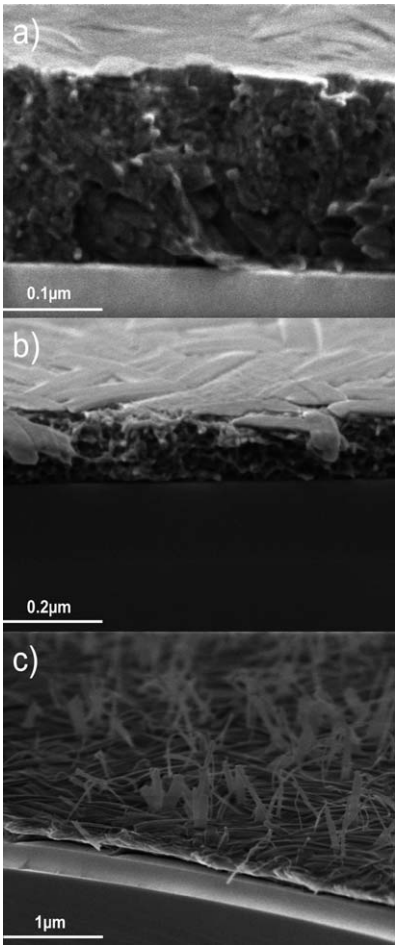

Fig. 5 Cross-sectional SEM images of thin films of P3HT:PDI-1 blends with the weight ratios of (a) 1 : 3, (b) 1 : 1, and (c) 3 : 1.

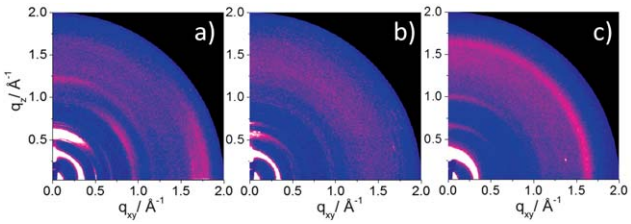

Fig. 6 GIWAXS patterns of thin films of P3HT:PDI-1 blends with the weight ratios of (a) 1 : 3, (b) 1 : 1, and (c) 3 : 1.

corresponding phases, GIWAXS of the blended layers was performed and compared to the pure compounds (Fig. 6). The analysis of the patterns indicates molecular reorganization in some of the blends, but at the same time does not allow the FET results to be fully explained. Surprisingly for the P3HT:PDI-1 1 : 1 blend, a balanced ambipolar transport is observed with mobilities of $\mu_h = 4.5 \times 10^{-3}$ cm^2 V^{-1} s^{-1} and $\mu_e = 6 \times 10^{-3}$ cm^2 V^{-1} s^{-1} (Fig. 6b), despite molecular interactions as indicated by the absence of characteristic π-stacking reflections. These results indicate a higher influence of the phase separated microstructure on the device performance. Nevertheless, the equatorial (along q_z for $q_{x,y} = 0$) and meridional (along $q_{x,y}$ for $q_z = 0$) integrations in the q range between 0.3 Å^{-1} and 1.1 Å^{-1} confirm supramolecular structures of the pure compounds and thus phase separation. On the other hand, equatorial reflections for P3HT:PDI-1 3 : 1 are attributed only to the polymer suggesting low order of PDI-1 at this ratio. This is in line with the decrease in electron transport and the microstructure observation in which small PDI crystals stick out of the film. Interestingly, the arrangement of the P3HT backbone changes from a face-on in the pure state to an edge-on in the blend of P3HT:PDI-1 3 : 1 as evident from meridional π-stacking scattering intensities and equatorial reflections related to the chain-to-chain spacing (Fig. S1†). Additionally, the π-stacking distance slightly decreases from 3.80 Å for pure P3HT to 3.70 Å in the mixture (Fig. S1†). However, the nearly uniform azimuthal distribution of this reflection would suggest a random arrangement of the backbone towards the surface. This might be an additional reason for the drop in hole mobility in the blend.

In the P3HT:PDI-1 1 : 3 film the polymer backbones are oriented edge-on while PDI-1 adapts an identical organization as in the pure state. Thereby, in the scattering pattern a double meridional reflection with maxima located at the positions corresponding to real-space distances of 3.60 Å and 3.40 Å is visible. The smaller value may be assigned to the π-stacking of PDI-1, while 3.60 Å can be attributed to a decreased packing distance of P3HT. At the moment, the driving force for tighter packing of P3HT in the blend is unclear.

To conclude, the analysis of GIWAXS patterns confirms the phase separation between both compounds since only spacings for pure P3HT and PDI-1 emerge. In the blend a reorganization of P3HT to an edge-on arrangement is observed. As already mentioned above, it is not possible to correlate the molecular order to the device performance. This indicates a more important influence of the film microstructure on the charge carrier transport than the organization of the molecules within the phases.

For the P3HT and PDI-2 (1 : 3, 1 : 1 and 3 : 1) blends, the charge carrier mobilities were also determined from the transfer curves (Fig. 7). For the blend with the highest acceptor concentration (P3HT:PDI-2 1 : 3), hole and electron mobilities of $\mu_h = 7 \times 10^{-3}$ cm^2 V^{-1} s^{-1} and $\mu_e = 2 \times 10^{-3}$ cm^2 V^{-1} s^{-1} were derived from the transfer curves (Fig. 7a). As already observed for the P3HT:PDI-1 system, the electron mobility is significantly enhanced for PDI-2 in the blend in comparison to the pure acceptor (10^{-8} cm^2 V^{-1} s^{-1}), while for the same film the

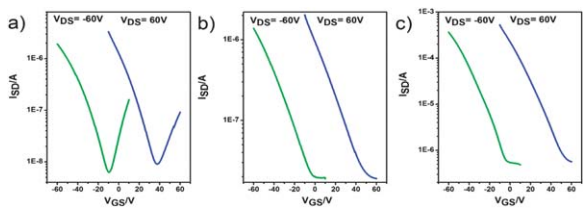

Fig. 7 Transfer FET characteristics for the P3HT:PDI-2 blend: (a) 1 : 3, (b) 1 : 1, and (c) 3 : 1.

Open Access Article. Published on 29 January 2013. Downloaded on 12/15/2025 9:26:05 AM.
This article is licensed under a Creative Commons Attribution 3.0 Unported Licence.

hole mobility drops half order of magnitude to that of pure P3HT (Table 1). The crossover point from the electron- to hole-dominated current in the negative drain mode ($V_{DS} < 0$) is slightly shifted to *ca.* $V_g = -10$ V (Fig. 7a). At the same time in the positive V_{DS} regime, domination of the electron transport becomes obvious from $V_g > 40$ V which is higher than for the 1 : 1 P3HT:PDI-1 blend.

The increase of the donor fraction in the active layer to a blend ratio of 1 : 1 and 3 : 1 P3HT:PDI-2 shows no electron transport. This is also evident from the asymmetric transfer plots in Fig. 7b and c. Only a hole mobility of $\mu_h = 2 \times 10^{-3}$ cm^2 V^{-1} s^{-1} is determined for 1 : 1 P3HT:PDI-2 and $\mu_h = 0.1$ cm^2 V^{-1} s^{-1} for 3 : 1 P3HT:PDI-2. The latter value is surprisingly two orders of magnitude higher than that for the pure polymer. It seems that a minor concentration of an n-type small molecule semiconductor acceptor can improve the performance of the p-type polymer in the major matrix. The reason for the higher hole transport for the blend of P3HT:PDI-2 3 : 1 might be doping of P3HT by the addition of a small amount of PDI-2. Recently, successful doping of P3HT with the strong acceptor 3,5,6-tetrafiuoro-7,7,8,8-tetracyanoquinodimethane (4-TCNQ) has been reported. The incorporation of TCNQ resulted in hole mobilities higher by a factor of 30 in comparison to pure P3HT, while the threshold voltage was controllable by adjustment of the doping concentration.[26] However, we expect such a doping effect of PDI-2 to be relatively small since the improvement in hole mobility occurs only for the P3HT:PDI-2 3 : 1 ratio. Another explanation could be the reorganization of P3HT in the blend allowing a 3D charge transport (see below).

The microstructure was studied firstly by AFM and is presented in Fig. S3.† In all three blend ratios, large crystals on top of the film are observed which are assigned to PDI-2. This is similar to the observations made for the PDI-1 blends. In comparison to the pure acceptor, the crystal microstructure of PDI-2 is significantly changed in the presence of P3HT. In the blended layers, long crystals are grown with a length of up to 1.5 μm, which are similar to PDI-1 in the mixture. However, the crystal size seems to be independent of the blend ratio since the smallest dimensions are observed for the equivalent blend. Therefore, the film topography does not fully explain the differences in device performance. Although the device characteristics of P3HT:PDI-2 with 1 : 3 (Fig. 7a) and 3 : 1 (Fig. 7c) ratios significantly differ, the PDI-2 crystals on top of the layer show almost identical microstructures. More insight into the phase separated film is obtained by SEM which reveals a diagonal penetration of the elongated single crystals through the entire film for P3HT:PDI-2 3 : 1 (Fig. 8b). In this way, the crystals are not interconnected and do not create the necessary network for the charge carrier percolation pathways. We assume that this microstructure is due to the lower tendency of PDI-2 to crystallize. However, the organization is different for the 1 : 3 P3HT:PDI-2 blend, for which the SEM shows a bilayer with a distinct horizontal phase separation between the donor and acceptor (Fig. 8a). In such microstructures both phases form the required conduction layers for individual charge carriers. Flat, tightly packed and interconnected networks of PDI-2 crystals form the pathways for electrons.

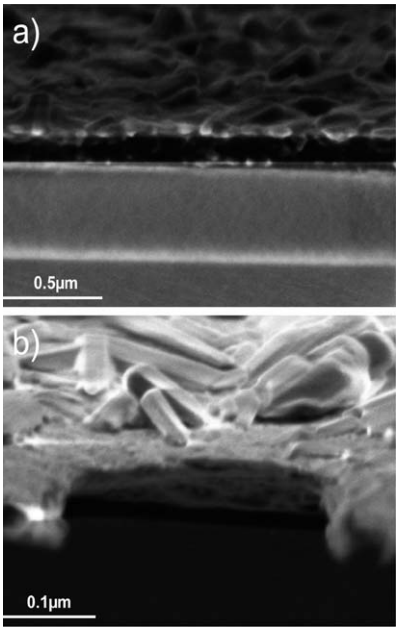

Fig. 8 Cross-sectional SEM images of thin films of P3HT:PDI-2 blends with the weight ratios of (a) 1 : 3 and (b) 3 : 1.

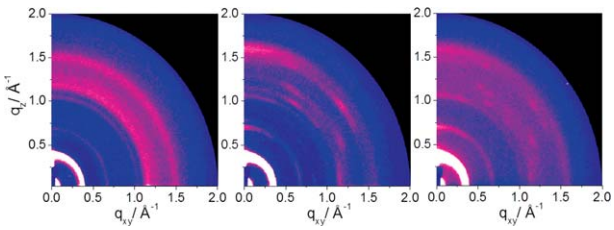

Fig. 9 GIWAXS patterns of thin films of P3HT:PDI-2 blends with the weight ratios of (a) 1 : 3, (b) 1 : 1, and (c) 3 : 1.

The GIWAXS data confirm a separated crystallization of P3HT and PDI-2 in the blends (Fig. 9). This is especially obvious from small-angle reflections indicating both types of structures in the blended layer (Fig. S1†). The high hole mobility of 0.1 cm^2 V^{-1} s^{-1} of P3HT:PDI-2 3 : 1 is attributed to the organization of P3HT in the blend film (Fig. 9c). The π-stacking reflection is relatively isotropic with an intensity maximum on the meridian suggesting the preferred face-on orientation, while peaks related to the chain-to-chain spacing also appear in the meridional plane which is typical for the edge-on arrangement. This, again, might be an indication for a simultaneous edge-on and face-on organization of P3HT towards the surface, which allows an enhanced 3D charge carrier transport. In contrast to pure P3HT, which organizes in an identical manner (Fig. 2a), the edge-on fraction of the polymer in the blend is well packed as evident from corresponding meridional π-stacking reflections ensuring an unhindered charge transport (Fig. 9c). Similar phenomena have been observed for high performance isoindigo-based polymers.[27] It is also interesting that the addition of a minor amount of PDI leads to a rearrangement of P3HT in the blend (for P3HT:PDI 3 : 1 blends). This would suggest that

 This journal is © The Royal Society of Chemistry 2013

Open Access Article. Published on 29 January 2013. Downloaded on 12/15/2025 9:26:05 AM.
This article is licensed under a Creative Commons Attribution 3.0 Unported Licence.

the face-on and edge-on surface organization of the polymer backbone can be controlled by processing. A similar effect was observed for naphthobisthiadiazole-based polymers, which change the arrangement from edge-on in pure films to face-on in the presence of PCBM.[28] On the other hand, the GIWAXS pattern of P3HT:PDI-2 1 : 3 equals the one for pure PDI-2 displaying isotropic reflections which are characteristic for randomly arranged molecules towards the surface (Fig. 9a). Nevertheless, an improvement by five orders of magnitude in electron mobility was derived for this system.

To summarize the SEM and GIWAXS data for the P3HT:PDI-2 blends, analogous to P3HT:PDI-1, the ambipolar device behavior mainly depends on the phase separated microstructure. A horizontal phase separation leads to an ambipolar transistor response, while a film with embedded PDI crystals shows only a hole transport. The reorganization of P3HT from a pure face-on to a simultaneous edge-on and face-on arrangement significantly favors this hole migration through the active layer.

Conclusions

All investigated blends reveal a phase separation between the donor and acceptor with P3HT mainly at the HMDS interface and the PDI derivatives crystallized on top of the film. For solar cells this is the appropriate layer arrangement where the donor is located at the ITO electrode. In the transistor, a continuous phase of the donor and acceptor phase in the micrometer long channel is required. This is apparently not the case for all samples since not all devices show an ambipolar behavior, but all FETs reveal hole transport with mobilities depending on the composition. Due to variation in solubility and crystallization, the PDIs phase separate differently at equal blend compositions affecting the electron transport. While electron transport is observed only for a blend with excess of PDI-2, the corresponding compositions with PDI-1 lack negative charge carriers in the field-effect. Interestingly, the cross-sectional SEM images for the blend with an ambipolar device performance clearly exhibit a well-defined homogenous horizontal phase separation. In samples with only a hole transport, the PDI crystals are embedded within the polymer matrix and in this way they are not interconnected. These results are in line with the previous solar cell studies in which PDI-2 showed a slightly higher short circuit current due to the interdigitated heterostructure in comparison to PDI-1. The FET response is interesting since one could also assume that the position of the layer towards the dielectric is more crucial. Probably this is partly the case since a hole transport is determined in all devices by the main charge carrier pathway established at the near surface interface where the P3HT layer is positioned. These results are in line with more homogenous phase separated P3HT:PCBM films which do not show significant differences between bottom and top gate devices.[29]

This work provides further understanding of the influence of the microstructure on the transport mechanism in heterojunction ambipolar transistors based on a polymer–crystalline molecule blend. Another promising effect is the significant mobility increase in comparison to the pure compounds. This is a new observation for donor–acceptor composites and an attractive approach for the development of ambipolar heterojunction FETs. The enhancement in performance for the PDI derivatives is related to a decrease in crystallinity in the blend, while P3HT undergoes a structural reorganization providing 3D pathways for charge carriers. It is necessary to look into further binary blend systems to gain deeper understanding of the relationship between composition, microstructure, molecular organization and device performance.

Acknowledgements

The authors thank G. Glasser and I. Lieberwirth for the cross-sectional SEM images and also for helpful discussions. This work was financially supported by the ERC Advanced Grant NANOGRAPH (AdG-2010-267160), Australian Solar Institute (Fellowship for W. W. H. Wong and project grant), Australian Research Council (DP0877325), the AAS-BMBF Australia–Germany Solar Photovoltaic Research Exchange Program, the German Science Foundation (Korean–German IR TG), the European Community's Seventh Framework Programme ONE-P (grant agreement no. 212311), DFG Priority Program SPP 1355, DFG MU 334/32-1, DFG Priority Program SPP 1459, and ESF Project GOSPEL (Ref Nr: 09-EuroGRAPHENE-FP-001). A. Kiersnowski acknowledges the support from Marie Curie Intra European Fellowship (PIEF-GA-2009-253521) granted within 7th EU Framework program. The temperature dependent GIWAXS experiments were undertaken on the SAXS/WAXS beamline at the Australian Synchrotron, Victoria, Australia.

Notes and references

1 (*a*) A. C. Arias, J. D. MacKenzie, I. McCulloch, J. Rivnay and A. Salleo, *Chem. Rev.*, 2010, **110**, 3; (*b*) S.-J. Kim and J.-S. Lee, *Nano Lett.*, 2010, **10**, 2884.

2 (*a*) H. N. Tsao, D. M. Cho, I. Park, M. R. Hansen, A. Mavrinskiy, D. Y. Yoon, R. Graf, W. Pisula, H. W. Spiess and K. Müllen, *J. Am. Chem. Soc.*, 2011, **133**, 2605; (*b*) H. Yan, Z. Chen, Y. Zheng, C. Newman, J. R. Quinn, F. Dötz, M. Kastler and A. Facchetti, *Nature*, 2009, **457**, 679; (*c*) H. Chen, Y. Guo, G. Yu, Y. Zhao, J. Zhang, D. Gao, H. Liu and Y. Liu, *Adv. Mater.*, 2012, **24**, 4618.

3 F. S. Kim, X. Guo, M. D. Watson and S. Jenekhe, *Adv. Mater.*, 2010, **22**, 478.

4 (*a*) L.-L. Chua, J. Zaumseil, J.-F. Chang, E. C. W. Ou, P. K. H. Ho, H. Sirringhaus and R. H. Friend, *Nature*, 2005, **434**, 194; (*b*) J. Cornil, J.-L. Brédas, J. Zaumseil and H. Sirringhaus, *Adv. Mater.*, 2007, **19**, 1791.

5 (*a*) E. Gili, M. Caironi and H. Sirringhaus, *Appl. Phys. Lett.*, 2012, **100**, 123303; (*b*) K. J. Baeg, J. Kim, D. Khim, M. Caironi, D. Y. Kim, I. K. You, J. R. Quinn, A. Facchetti and Y. Y. Noh, *ACS Appl. Mater. Interfaces*, 2011, **3**, 3205; (*c*) H. Li, B. C.-K. Tee, G. Giri, J. W. Chung, S. Y. Lee and Z. Bao, *Adv. Mater.*, 2012, **24**, 2588.

6 (*a*) M. L. Tang, A. D. Reichardt, N. Miyaki, R. M. Stoltenberg and Z. Bao, *J. Am. Chem. Soc.*, 2008, **130**, 6664; (*b*) Z. Chen, M. J. Lee, R. S. Ashraf, Y. Gu, S. Albert-Seifried,

Open Access Article. Published on 29 January 2013. Downloaded on 12/15/2025 9:26:05 AM.
This article is licensed under a Creative Commons Attribution 3.0 Unported Licence.

M. M. Nielsen, B. Schroeder, T. D. Anthopoulos, M. Heeney, I. McCulloch and H. Sirringhaus, *Adv. Mater.*, 2012, **24**, 647; (*c*) Z. Chen, H. Lemke, S. Albert-Seifried, M. Caironi, M. M. Nielsen, M. Heeney, W. Zhang, I. McCulloch and H. Sirringhaus, *Adv. Mater.*, 2010, **22**, 2371; (*d*) J. D. Yuen, J. Fan, J. Seifter, B. Lim, R. Hufschmid, A. J. Heeger and F. Wudl, *J. Am. Chem. Soc.*, 2011, **133**, 20799; (*e*) S. Cho, J. Lee, M. Tong, J. H. Seo and C. Yang, *Adv. Funct. Mater.*, 2011, **21**, 1910; (*f*) J. C. Bijleveld, A. P. Zoombelt, S. G. J. Mathijssen, M. M. Wienk, M. Turbiez, D. M. de Leeuw and R. A. J. Janssen, *J. Am. Chem. Soc.*, 2009, **131**, 16616; (*g*) J. S. Lee, S. K. Son, S. Song, H. Kim, D. R. Lee, K. Kim, M. J. Ko, D. H. Choi, B. S. Kim and J. H. Cho, *Chem. Mater.*, 2012, **24**, 1316.

7 (*a*) J. Smith, R. Hamilton, I. McCulloch, N. Stingelin-Stutzmann, M. Heeney, D. D. C. Bradleya and T. D. Anthopoulos, *J. Mater. Chem.*, 2010, **20**, 2562; S. B. Jo, W. H. Lee, L. Qiu and K. Cho, *J. Mater. Chem.*, 2012, **22**, 4244.

8 (*a*) F. Dinelli, R. Capelli, M. A. Loi, M. Murgia, M. Muccini, A. Facchetti and T. J. Marks, *Adv. Mater.*, 2006, **18**, 1416; (*b*) J. Wang, H. Wang, X. Yan, H. Huang and D. Yan, *Appl. Phys. Lett.*, 2005, **87**, 093507; (*c*) R. Ye, M. Baba, Y. Oishi, K. Mori and K. Suzuki, *Appl. Phys. Lett.*, 2005, **86**, 253505; (*d*) J. G. Labram, P. H. Wöbkenberg, D. D. C. Bradley and T. D. Anthopoulos, *Org. Electron.*, 2010, **11**, 1250.

9 (*a*) M. A. Loi, C. Rost-Bietsch, M. Murgia, S. Karg, W. Riess and M. Muccini, *Adv. Funct. Mater.*, 2006, **16**, 41; (*b*) A. Babel, Y. Zhu, K. Cheng, W. Chen and S. Jenekhe, *Adv. Funct. Mater.*, 2007, **17**, 2542; (*c*) M. Shkunov, R. Simms, M. Heeney, S. Tierney and I. McCulloch, *Adv. Mater.*, 2005, **17**, 2608; (*d*) K. Szendrei, D. Jarzab, Z. Chen, A. Facchetti and M. A. Loi, *J. Mater. Chem.*, 2010, **20**, 1317; (*e*) E. J. Meijer, D. M. De Leeuw, S. Setayesh, E. van Veenendaal, B. H. Huisman, P. W. M. Blom, J. C. Hummelen, U. Scherf and T. M. Klapwijk, *Nat. Mater.*, 2003, **2**, 678; (*f*) Y. Matsuo, Y. Sato, T. Niinomi, I. Soga, H. Tanaka and E. Nakamura, *J. Am. Chem. Soc.*, 2009, **131**, 16048.

10 (*a*) C. J. Brabec, M. Heeney, I. McCulloch and J. Nelson, *Chem. Soc. Rev.*, 2011, **40**, 1185; (*b*) S. Günes, H. Neugebauer and N. S. Sariciftci, *Chem. Rev.*, 2007, **107**, 1324–1338.

11 C. J. Brabec, N. S. Sariciftci and J. C. Hummelen, *Adv. Funct. Mater.*, 2001, **11**, 15.

12 A. A. Virkar, S. Mannsfeld, Z. Bao and N. Stingelin, *Adv. Mater.*, 2010, **22**, 3857.

13 (*a*) X. Yang and J. Loos, *Macromolecules*, 2007, **40**, 1354; (*b*) M. Treier, J.-B. Arlin, C. Ruzi, Y. H. Geerts, V. Lemaur, J. Cornil and P. Samori, *J. Mater. Chem.*, 2012, **22**, 9509.

14 (*a*) M. T. Dang, L. Hirsch and G. Wantz, *Adv. Mater.*, 2011, **23**, 3597; (*b*) A. C. Mayer, S. R. Scully, B. E. Hardin, M. W. Rowell and M. D. McGehee, *Mater. Today*, 2007, **10**, 28.

15 V. Kamm, G. Battagliarin, I. A. Howard, W. Pisula, A. Mavrinskiy, C. Li, K. Müllen and F. Laquai, *Adv. Energy Mater.*, 2011, **1**, 297.

16 (*a*) J. Soeda, T. Uemura, Y. Mizuno, A. Nakao, Y. Nakazawa, A. Facchetti and J. Takeya, *Adv. Mater.*, 2011, **23**, 3681; (*b*) X. Zhan, A. Facchetti, S. Barlow, T. J. Marks, M. A. Ratner, M. R. Wasielewski and S. R. Marder, *Adv. Mater.*, 2011, **23**, 268 and references therein.

17 (*a*) Z. Wu, A. Petzold, T. Henze, T. Thurn-Albrecht, R. Lohwasser, M. Sommer and M. Thelakkat, *Macromolecules*, 2010, **43**, 4646; (*b*) O. F. Pascui, R. Lohwasser, M. Sommer, M. Thelakkat, T. Thurn-Albrecht and K. Saalwächter, *Macromolecules*, 2010, **43**, 9401.

18 A. Zen, J. Pflaum, S. Hirschmann, W. Zhuang, F. Jaiser, U. Asawapirom, J. P. Rabe, U. Scherf and D. Neher, *Adv. Funct. Mater.*, 2004, **14**, 757.

19 R. J. Kline, M. D. McGehee, E. N. Kadnikova, J. Liu and J. M. J. Fréchet, *Adv. Mater.*, 2003, **15**, 1519.

20 H. Sirringhaus, P. J. Brown, R. H. Friend, M. M. Nielsen, K. Bechgaard, B. M. W. Langeveld-Voss, A. J. H. Spiering, R. A. J. Janssen, E. W. Meijer, P. Herwig and D. M. de Leeuw, *Nature*, 1999, **401**, 685.

21 J. Rivnay, L. H. Jimison, J. E. Northrup, M. F. Toney, R. Noriega, S. Lu, T. J. Marks, A. Facchetti and A. Salleo, *Nat. Mater.*, 2009, **8**, 952.

22 (*a*) C. Liu, Z. Liu, H. T. Lemke, H. N. Tsao, R. C. G. Naber, Y. Li, K. Banger, K. Müllen, M. M. Nielsen and H. Sirringhaus, *Chem. Mater.*, 2010, **22**, 2120; (*b*) F. Nolde, W. Pisula, S. Müller, C. Kohl and K. Müllen, *Chem. Mater.*, 2006, **18**, 3715.

23 (*a*) E. Lim, B.-J. Jung, M. Chikamatsu, R. Azumi, K. Yase, L.-M. Do and H.-K. Shim, *Org. Electron.*, 2008, **9**, 952; (*b*) E. Orgiu, A. M. Masillamani, J.-O. Vogel, E. Treossi, A. Kiersnowski, M. Kastler, W. Pisula, F. Dötz, V. Palermo and P. Samorì, *Chem. Commun.*, 2012, **48**, 1562; (*c*) J. Smith, W. Zhang, R. Sougrat, K. Zhao, R. Li, D. Cha, A. Amassian, M. Heeney, I. McCulloch and T. D. Anthopoulos, *Adv. Mater.*, 2012, **24**, 2441.

24 (*a*) J. Smith, R. Hamilton, Y. Qi, A. Kahn, D. D. C. Bradley, M. Heeney, I. McCulloch and T. D. Anthopoulos, *Adv. Funct. Mater.*, 2010, **20**, 2330; (*b*) R. Hamilton, J. Smith, S. Ogier, M. Heeney, J. E. Anthony, I. McCulloch, D. D. C. Bradley, J. Veres and T. D. Anthopoulos, *Adv. Mater.*, 2009, **21**, 1166; (*c*) J. L. Li, M. Kastler, W. Pisula, J. W. F. Robertson, D. Wasserfallen, A. C. Grimsdale, J. S. Wu and K. Müllen, *Adv. Funct. Mater.*, 2007, **17**, 2528.

25 N. D. Treat, M. A. Brady, G. Smith, M. F. Toney, E. J. Kramer, C. J. Hawker and M. L. Chabinyc, *Adv. Energy Mater.*, 2011, **1**, 82.

26 (*a*) L. Ma, W. H. Lee, Y. D. Park, J. S. Kim, H. S. Lee and K. Cho, *Appl. Phys. Lett.*, 2008, **92**, 063310; (*b*) Y. M. Zhang and P. W. Blom, *Appl. Phys. Lett.*, 2010, **97**, 083303; (*c*) K.-H. Yim, G. L. Whiting, C. E. Murphy, J. J. M. Halls, J. H. Burroughes, R. H. Friend and J.-S. Kim, *Adv. Mater.*, 2008, **20**, 3319.

27 J. Mei, D. H. Kim, A. L. Ayzner, M. F. Toney and Z. Bao, *J. Am. Chem. Soc.*, 2011, **133**, 20130.

28 I. Osaka, M. Shimawaki, H. Mori, I. Doi, E. Miyazaki, T. Koganezawa and K. Takimiya, *J. Am. Chem. Soc.*, 2012, **134**, 3498.

29 J. G. Labram, E. B. Domingo, N. Stingelin, D. D. C. Bradley and T. D. Anthopoulos, *Adv. Funct. Mater.*, 2011, **21**, 356.

 This journal is © The Royal Society of Chemistry 2013